HHDevelopment 130, 1877-1887

doi:10.1242/dev.00411

Strabismus requires Flamingo and Prickle function to regulate tissue polarity in the *Drosophila* eye

Amy S. Rawls and Tanya Wolff[1]

Department of Genetics, Washington University School of Medicine, St. Louis, MO 63110, USA
*Author for correspondence (e-mail: twolff@genetics.wustl.edu)

Accepted 27 January 2003

SUMMARY

Tissue polarity in *Drosophila* is regulated by a number of genes that are thought to function in a complex, many of which interact genetically and/or physically, co-localize, and require other tissue polarity proteins for their localization. We report the enhancement of the *strabismus* tissue polarity phenotype by mutations in two other tissue polarity genes, *flamingo* and *prickle*. Flamingo is autonomously required for the establishment of ommatidial polarity. Its localization is dynamic throughout ommatidial development and is dependent on Frizzled and Notch. Flamingo and Strabismus co-localize for several rows posterior to the morphogenetic furrow and subsequently diverge. While neither of these proteins is required for the other's localization, Prickle localization is influenced by Strabismus function. Our data suggest that Strabismus, Flamingo and Prickle function together to regulate the establishment of tissue polarity in the *Drosophila* eye.

Key words: Tissue polarity, *strabismus*, *flamingo*, Cadherin, *prickle*, *Drosophila* eye

INTRODUCTION

The organization of tissues and organs based upon a precise body plan is a universal theme in metazoan development. Polarity within a cell is essential for cells to perform specialized functions. Similarly, the polarized orientation of cells within an epithelium, a phenomenon known as tissue, epithelial, or planar cell polarity, shapes the tissue into a functional organ. Until recently, genes regulating these processes have been studied almost exclusively in *Drosophila*. The proteins encoded by these tissue polarity genes impose a high degree of order in a variety of epithelial structures, including the uniform orientation of bristles and hairs throughout the adult body, the polarized organization of tarsi in the legs, and the precise patterning of unit eyes, or ommatidia, in the compound eye. A growing number of tissue polarity genes are being identified, yet the mechanisms by which the proteins encoded by these genes function and the intricate network of interactions that connects these genes are poorly understood.

We have identified interactions between a subset of tissue polarity genes in the developing *Drosophila* eye. The compound eye of the fly is a polarized epithelium composed of approximately 800 unit eyes, or ommatidia. Each ommatidium contains 20 cells, including eight photoreceptors (R1-R8). The photosensitive organelles of the photoreceptors, the rhabdomeres, are arranged in a characteristic trapezoid in which photoreceptor R3 defines the 'point' of the trapezoid. There are two chiral forms of the trapezoid and they fall on opposite sides of a dorsal-ventral midline known as the equator. In the dorsal hemisphere of the eye, the points of the trapezoids face the dorsal margin while those in the ventral half face the ventral margin of the eye (Fig. 1A).

This highly ordered adult pattern is established in the eye imaginal disc of the third larval instar. Initially, nascent photoreceptor clusters are uniformly oriented within this epithelium. An essential step in polarizing the retinal epithelium is a break in symmetry between the future photoreceptors R3 and R4 as they adopt distinct cell fates. The photoreceptor clusters subsequently rotate 90° within the epithelium – they rotate counterclockwise in the dorsal half and clockwise in the ventral half of the eye (reviewed by Wolff and Ready, 1993).

A number of tissue polarity genes have been identified, among them *frizzled* (*fz*), *prickle* (*pk*), *dishevelled* (*dsh*), *diego* (*dgo*), *strabismus* (*stbm*; also known as *Van Gogh*) and *flamingo* (*fmi*; also known as *starry night*) (Zheng et al., 1995; Gubb et al., 1999; Klingensmith et al., 1994; Feiguin et al., 2001; Wolff and Rubin, 1998; Taylor et al., 1998; Usui et al., 1999; Chae et al., 1999). We have focused our efforts on identifying the position of *stbm* in the tissue polarity pathway as a means of more precisely defining its role in setting up polarity in the eye. Flies null for *stbm* lack an equator because of a variety of defects in ommatidial orientation and fate mis-specification (Wolff and Rubin, 1998). *stbm* acts cell-autonomously to define R4 (Wolff and Rubin, 1998), and it co-localizes with other tissue polarity proteins at the contact between photoreceptors R3 and R4 (this report) (Strutt et al., 2002).

To identify genes that interact with *stbm*, we carried out a

genetic modifier screen. We identified two tissue polarity genes, *fmi* and *pk*, that dominantly modify the *stbm* mutant phenotype. The role of *fmi* in tissue polarity was identified from its requirement for polarization of wing hairs (Usui et al., 1999). *fmi* also plays an essential role in the first asymmetric cell division of the SOP cell lineage in the PNS (Lu et al., 1999). *fmi* encodes a protein with a seven-pass transmembrane domain, a unique cytoplasmic tail and nine extracellular cadherin domains (Usui et al., 1999; Chae et al., 1999). The extracellular cadherin domains are capable of mediating cell-cell adhesion while the unique intracellular domain is potentially involved in signal transduction (Usui et al., 1999).

In this paper, we define a role for *fmi* in directing tissue polarity in the *Drosophila* retina. We show that loss-of-function *fmi* interacts genetically with both misexpression and loss-of-function *stbm*. We have generated an antibody against Stbm and show that Stbm is apically localized in all cells anterior to, in, and several rows posterior to, the morphogenetic furrow. Stbm subsequently fades in R8, R2 and R5 and becomes pronounced at the contact between R3 and R4 [also reported using Sbm-YFP by Strutt et al. (Strutt et al., 2002)]. We also show that Fmi and Stbm co-localize in early, but not later, stages of ommatidial development. In addition, we show that *fmi* is cell- and ommatidium-autonomously required for ommatidial polarity [as also reported by others (Yang et al., 2002; Das et al., 2002; Strutt et al., 2002)].

Like *fmi*, *pk* also acts globally to influence polarity throughout the fly (reviewed by Mlodzik, 2000). Pk has several protein interaction domains and binds Dsh (Tree et al., 2002). Tree et al. have suggested this interaction is an essential component of a feedback loop that asymmetrically localizes Fz and Dsh in wing cells, ultimately leading to the polarized arrangement of hairs and bristles. Similarly, in the eye, *pk* is essential in establishing Fz asymmetry in R3 and R4 (Strutt et al., 2002). Taylor et al. have demonstrated a genetic interaction between *pk* and *stbm* in the wing (Taylor et al., 1998). Here we show that *pk* enhances both misexpression and loss-of-function *stbm* phenotypes in the eye, and that localization of Pk is disrupted in *stbm* mutant ommatidia.

MATERIALS AND METHODS

Genetics and deficiency screen

Fly strains used: *sev-stbm*$^{14\text{-}1}$, *stbm*^{153}, *stbm*^{6cn}, FRT42, *fmi*^{192}/CyO (a genetic null allele identified in a screen for novel tissue polarity mutants, T. Wolff, unpublished), *fmi*^{frz3} (a gift from D. Gubb), *fmi*^{E59} (a gift from T. Uemura), *w*,hsFLP122;FRT42, *ey*GAL4, UASFLP;FRT42 GMR*hid*, *shi*^{2ts}, *hk*^{11} (a gift from H. Kramer), *fz*^{KD4A}, *N*^{ts1}, *pk*^{pk1}, *pk*^{eq} (a gift from T. Xu). Unless otherwise noted, phenotypic analyses were conducted using FRT42*fmi*^{192}. *fmi*^{192} mosaic clones were generated using heat shock-induced, FLP/FRT-mediated recombination (Xu and Rubin, 1993). Entirely mutant *fmi* eyes were generated using the *EGUF* (*eyeless*-Gal4 UAS-FLP) system of recombination (Stowers and Schwarz, 1999), a modification of the FLP-FRT system in which recombination is driven selectively in the eye by the *eyeless* promoter and wild-type cells are killed by the expression of GMR-*hid* and uncharacterized cell lethal mutations.

sev-stbm homozygous flies were crossed to the 250 second and third chromosome deletion lines that constitute the Bloomington Deficiency Kit. The degree of eye roughness in F1 transheterozygotes was analyzed under the dissecting microscope and compared to that of *sev-stbm* heterozygotes. A secondary screen, in which adult eyes were fixed and sectioned (as described by Wolff, 2000) and the phenotype quantified, was conducted on 27 candidate interactors. Six enhancers of *sev-stbm* were confirmed.

Phenotypic analyses

Adult eyes were fixed, embedded and sectioned according to standard protocol (Wolff, 2000). The number of ommatidia and eyes scored is as follows: Df(2R)E3363/*sev-stbm*$^{14\text{-}1}$: 383 ommatidia from 5 eyes; Df(2R)Jp4/*sev-stbm*$^{14\text{-}1}$: 480 ommatidia from 3 eyes; Roote 276/*sev-stbm*$^{14\text{-}1}$: 533 ommatidia from 3 eyes; Roote 2-42/*sev-stbm*$^{14\text{-}1}$: 557 ommatidia from 3 eyes; Df(2L)s1402/*sev-stbm*$^{14\text{-}1}$: 608 ommatidia from 3 eyes; Df(2R)pk78k/*sev-stbm*$^{14\text{-}1}$: 497 ommatidia from 3 eyes; *fmi*^{frz3}/*sev-stbm*$^{14\text{-}1}$: 1135 ommatidia from 14 eyes; *fmi*^{192}/*sev-stbm*$^{14\text{-}1}$: 877 ommatidia from 15 eyes; *fmi*^{E59}/*sev-stbm*$^{14\text{-}1}$: 872 ommatidia from 12 eyes; *fmi*^{frz3}/*fmi*^{frz3}: 1788 ommatidia from 17 eyes; *stbm*^{153},*fmi*^{frz3}/*stbm*^{153},*fmi*^{frz3}: 1024 ommatidia from 15 eyes; *stbm*^{153},+/*stbm*^{153},*fmi*^{frz3}: 1123 ommatidia from 16 eyes; +,*fmi*^{frz3}/*stbm*^{153},*fmi*^{frz3}: 976 ommatidia from 10 eyes; *EGUF-fmi*^{192}: 1612 ommatidia from 18 eyes; *fmi*^{192}/*fmi*^{192} mosaic clones: 792 ommatidia from 23 clones in 23 eyes; *pk*^{pk1}/*sev-stbm*$^{14\text{-}1}$: 1030 ommatidia from 11 eyes; and *pk*^{pk1}, *stbm*^{153}/*pk*^{pk1}, *stbm*^{153}: 729 ommatidia from 7 eyes.

Antibody generation

The anti-Stbm polyclonal antibody was raised against the N-terminal 143 amino acids of the protein. A 429 base pair PCR product was generated and subcloned in frame into the *Eco*RI/*Xho*I site of pGEX-4T-1 (Pharmacia). The fusion protein was purified on glutathione-agarose beads and used to immunize rabbits. Immunization and subsequent production were carried out by Pocono Rabbit Farm and Laboratory, Inc.

Immunohistology

Third instar larval eye discs were dissected and processed as described previously (Wolff, 2000). Tissue was incubated in primary antibody overnight at 4°C at concentrations of 1:10 for anti-Fmi [mouse monoclonal; generous gift from T. Uemura (Usui et al., 1999)], 1:600 for anti-Pk [rabbit polyclonal; generous gift from D. Tree and J. Axelrod (Tree et al., 2002)], 1:500 for anti-Stbm (rabbit polyclonal, see above) and 1:10 for anti-Armadillo (Arm) antibody (mouse monclonal, Developmental Studies Hybridoma Bank). Secondary antibodies conjugated to Alexafluor fluorescent dyes were used (Molecular Probes).

Fmi localization was studied in *fz*^{KD4A} null larval escapers. For immunostaining of Fmi in *shi*^{2ts} animals, third instar larvae were heat shocked at 31°C for 1 hour, eye discs removed and fixed immediately and immunostained as described above. Recovery experiments were conducted by allowing the larvae to recover at room temperature for 1, 2 or 6 hours following heat shock.

pk^{eq} has not been characterized at the molecular level, however it fails to complement known *pk*$^{pk\text{-}sple}$ alleles. This allele was chosen over *pk*^{pk1} to characterize Stbm localization because it produces an obvious eye phenotype, unlike the *pk*^{pk1} allele.

Fluorescent images were collected using a Leica TCS SP2 confocal microscope.

RESULTS

fmi and *stbm* interact genetically

The Bloomington deficiency kit was screened to identify genes that interact with the tissue polarity gene, *stbm*. The screen was carried out in a misexpression *stbm* background in which the *sevenless* (*sev*) promoter was used to drive expression of *stbm* (*sev-stbm*) in photoreceptors R3, R4 and R7 and the four cone cells. The phenotype of eyes of flies

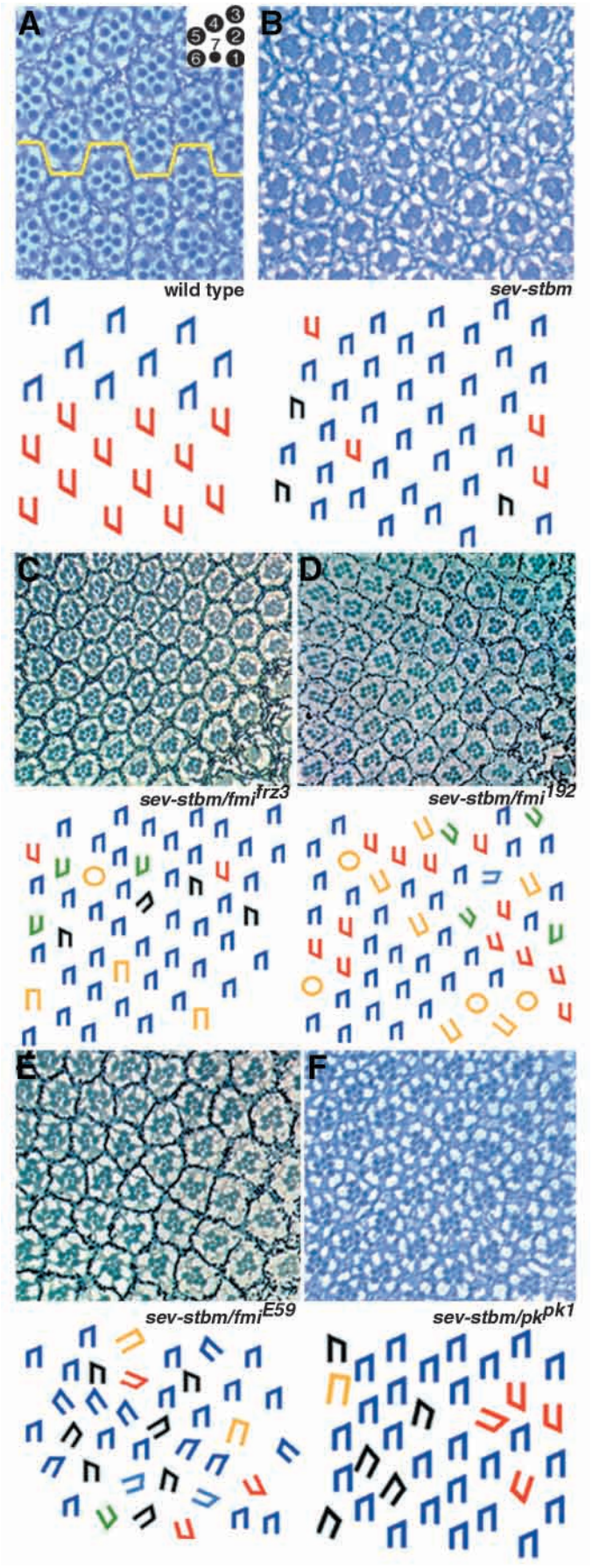

Fig. 1. *fmi* and *pk* mutations dominantly modify the *sev-stbm* eye phenotype. Tangential sections through adult eyes are shown in the top part of each panel and a schematic is given below, in which different chiral forms are shown in different colors. (A) In wild-type adult eyes, ommatidia in the dorsal hemisphere are oriented towards the dorsal pole while those in the ventral hemisphere are oriented towards the ventral pole. These fields of opposing ommatidial chirality are separated by the equator (yellow line). The inset illustrates the position of photoreceptors R1-R8 in a single ommatidium. (B-E) All sections are from the dorsal half of the eye. (B) *sev-stbm*. About 10% of ommatidia display errors in polarity, as illustrated by differently colored trapezoids. (C,D,E) Mutations in *fmi* enhance the *sev-stbm* phenotype. (C) *sev-stbm*/+*; fmi*^{frz3}/+, (D) *sev-stbm*/+*; fmi*^{192} /+, (E) *sev-stbm* /+*; fmi*^{E59}/+. Three *fmi* alleles, *fmi*^{frz3} (a hypomorphic allele), *fmi*^{192} and *fmi*^{E59} (both null alleles) dominantly enhance the *sev-stbm* phenotype about 3 fold. Yellow forms in the schematics denote symmetrical defects. (F) A hypomorphic *pk* allele, *pk*^{pk1}, enhances the *sev-stbm* phenotype about 2.5 fold. (See Table 1 for quantitative data.) Blue and red trapezoids represent ommatidia in the dorsal and ventral hemispheres, respectively. Anterior to the right.

carrying the *sev-stbm* transgene mimics the loss-of-function *stbm* phenotype, although it is milder (Wolff, unpublished): in transgenic flies carrying a single copy of *sev-stbm*, 10% of ommatidia exhibit disruptions in polarity (Fig. 1B). Externally, these eyes appear mildly rough, so both enhancement and suppression of this phenotype can be readily detected on the surface of the eye.

In an F_1 genetic modifier screen, 250 deletion lines from the Bloomington deficiency kit, which uncover approximately 70-75% of the second and third chromosomes (Berkeley *Drosophila* Genome Project), were crossed to *sev-stbm* and the progeny scored for dominant modification of the *sev-stbm* phenotype. Six deficiency lines were identified as dominant enhancers of the *sev-stbm* phenotype (Table 1); no suppressors were identified. We have identified the interacting gene in two of these six deletions (Bloomington deficiencies Df(2R)E3363 and Roote 276).

Df(2R)E3363, which uncovers chromosomal region 47A-47F, enhances the *sev-stbm* phenotype three-fold, increasing the percentage of ommatidia with polarity defects from 10% to 31% (Table 1). The most likely candidate for interaction within this region was a second tissue polarity gene, *fmi*, which maps to 47B4. To determine if *fmi* was the gene responsible for enhancement of the *sev-stbm* phenotype, three alleles, *fmi*^{frz3} (a hypomorph), *fmi*^{192} and *fmi*^{E59} (genetic nulls) were crossed to *sev-stbm*. These three alleles dominantly enhance the *sev-stbm* phenotype to the same extent as the original deficiency (Fig. 1C-E; Table 2), suggesting that *fmi* is the interacting locus.

Genetic interactions in a misexpression background can be unreliable, as the observed effect may be the consequence of, for example, non-specific effects on the promoter. To definitively demonstrate that *fmi* interacts genetically with *stbm*, the interaction was confirmed in a *stbm* loss-of-function background in which a recombinant line carrying the hypomorphic alleles *stbm*^{153} and *fmi*^{frz3}was analyzed. The *fmi*^{frz3} phenotype is dominantly enhanced approximately threefold in *stbm*^{153}, *fmi*^{frz3}/+, *fmi*^{frz3} flies, confirming the misexpression result (Fig. 2A,B; Table 3). In contrast, the

Table 1. *sev-stbm* (*ss*) is dominantly enhanced by six deficiency lines

Polarity defect	$ss^{14\text{-}1}$/Df(2R)E3363 (47A13-47E10)	$ss^{14\text{-}1}$/Roote 276 (42E4-43E7)	$ss^{14\text{-}1}$/Roote 2-42 (29C1-30C9)	$ss^{14\text{-}1}$/Df(2L)s1402 (30C)	$ss^{14\text{-}1}$/Df(2R)pk78k (42E3-43C3)	$ss^{14\text{-}1}$/Df(2R)Jp4 (51F13-52F9)
AP	37 (9.7%)	19 (3.6%)	36 (6.5%)	33 (5.4%)	38 (7.6%)	30 (6.3%)
DV	38 (9.9%)	48 (9.0%)	65 (11.7%)	27 (4.4%)	42 (8.5%)	44 (9.2%)
AP+DV	16 (4.2%)	7 (1.3%)	3 (0.5%)	12 (2.0%)	9 (1.8%)	17 (3.5%)
R3/R3	26 (6.8%)	66 (12.4%)	102 (18.3%)	30 (4.9%)	52 (10.5%)	27 (5.6%)
R4/R4	1 (0.3%)	1 (0.2%)	1 (0.2%)	4 (0.7%)	18 (3.6%)	5 (1.0%)
Total errors	118 (31.0%)	141 (26.5%)	207 (37.2%)	106 (17.4%)	159 (32.0%)	123 (25.6%)
n	383	533	557	608	497	480

Table 2. *sev-stbm* (*ss*) is dominantly enhanced by *fmi* and *pk* loss-of-function alleles

Polarity defect	$ss^{14\text{-}1}$/+	$ss^{14\text{-}1}/fmi^{frz3}$	$ss^{14\text{-}1}/fmi^{192}$	$ss^{14\text{-}1}/fmi^{E59}$	$ss^{14\text{-}1}/pk^{pk1}$
AP	22 (4.0%)	96 (8.5%)	62 (7.1%)	85 (9.7%)	72 (7.0%)
DV	32 (5.9%)	116 (10.2%)	116 (13.2%)	95 (10.9%)	85 (8.3%)
AP+DV	3 (0.5%)	53 (4.7%)	39 (4.4%)	25 (2.9%)	35 (3.4%)
R3/R3	4 (0.7%)	38 (3.3%)	17 (1.9%)	28 (3.2%)	56 (5.4%)
R4/R4	2 (0.4%)	14 (1.2%)	4 (0.5%)	8 (0.9%)	39 (3.8%)
Fail to rotate	–	15 (1.3%)	13 (1.5%)	7 (0.8%)	–
Total errors	63 (11.5%)	332 (29.3%)	251 (28.6%)	248 (28.4%)	287 (27.9%)
n	547	1135	877	872	1030

Table 3. Loss-of-function *stbm* interacts genetically with *fmi* and *pk* alleles

Polarity defect	fmi^{frz3}/fmi^{frz3}	$stbm^{153}/stbm^{153}$	$stbm^{153}$, fmi^{frz3}/+, fmi^{frz3}	$stbm^{153}$, $fmi^{frz3}/stbm^{153}$, fmi^{frz3}	pk^{pk1}, $stbm^{153}/pk^{pk1}$, $stbm^{153}$
AP	81 (4.5%)	116 (9.6%)	70 (7.2%)	124 (12.1%)	146 (20.0%)
DV	83 (4.6%)	240 (20.0%)	135 (13.8%)	185 (18.1%)	91 (12.5%)
AP+DV	45 (2.5%)	51 (4.2%)	59 (6.0%)	28 (2.7%)	14 (1.9%)
R3/R3	34 (1.9%)	17 (1.4%)	26 (2.7%)	161 (15.7%)	60 (8.2%)
R4/R4	3 (0.2%)	14 (1.2%)	18 (1.8%)	83 (8.1%)	51 (7.0%)
Fail to rotate	3 (0.2%)	41 (3.4%)	4 (0.4%)	16 (1.6%)	–
Missing Rs	–	–	9 (0.9%)	55 (5.4%)	–
Total errors	249 (13.9%)	479 (39.8%)	321 (32.9%)	652 (63.7%)	362 (49.7%)
n	1788	1203	976	1024	729

presence of a single copy of fmi^{frz3} in a $stbm^{153}$ homozygous background has no effect on the $stbm^{153}$ phenotype (data not shown). Phenotypes that are never seen in fmi^{frz3} or $stbm^{153}$ homozygotes appear in the double homozygotes. In these flies, viability drops from 100% to about 5%, there is a significant increase in the number of symmetric ommatidia (both R3/R3 and R4/R4), and lastly, some ommatidia are missing photoreceptors (Table 3).

fmi regulates ommatidial polarity

Consistent with its previously characterized roles in establishing polarity in cuticular structures, we report that *fmi* is also required to establish ommatidial polarity. The *fmi* mutant eye phenotype resembles that of previously described tissue polarity mutants, such as *fz*, *pk*, *dsh*, *dgo* and *stbm* (Zheng et al., 1995; Gubb et al., 1999; Klingensmith et al., 1994; Feiguin et al., 2001; Wolff and Rubin, 1998). Since null *fmi* alleles are lethal, we examined the mutant phenotype in FLP/FRT-generated clones and found that 37% of genetically mutant or mosaic ommatidia exhibit disrupted polarity (Fig. 3A,B; Table 4). The majority of mutant ommatidia display inversions on the anterior-posterior (AP) axis and the dorsal-ventral (DV) axis, although ommatidia that are inverted on both their AP and DV axes, as well as partially rotated ommatidia, symmetrical ommatidia (both R3/R3 and R4/R4) and unrotated ommatidia, are also present. It is interesting to note that the phenotype is stronger in clones that lie on or very close to the equator (Fig. 3B). Recently, the *fmi* eye polarity phenotype was also reported by others (Yang et al., 2002; Das et al., 2002; Strutt et al., 2002). The data reported here are qualitatively consistent with data presented in these reports.

The phenotype described above is similar to that seen in eyes entirely mutant for *fmi* (Fig. 3C, Table 4). Furthermore, the phenotype of the viable hypomorphic allele fmi^{frz3} is similar to, but weaker than, that described for null alleles (Fig. 2A; Table 3).

Das et al. (Das et al., 2002) reported that fmi^{E59} mutant clones have a cell death phenotype in which 20% of *fmi* ommatidia lack photoreceptors. This is in contrast to observations that neither fmi^{E45}/fmi^{E59} transheterozygotes (Strutt et al., 2002) nor ommatidia in fmi^{192} clones (reported here) exhibit a photoreceptor death phenotype. While the basis of this difference is not known, it is interesting that *stbm*, *fmi* double homozygotes are missing photoreceptors (Table 3), perhaps suggesting a previously unrecognized role for these loci in photoreceptor specification or survival. [A small percentage of ommatidia are missing photoreceptors in *EGUF-*

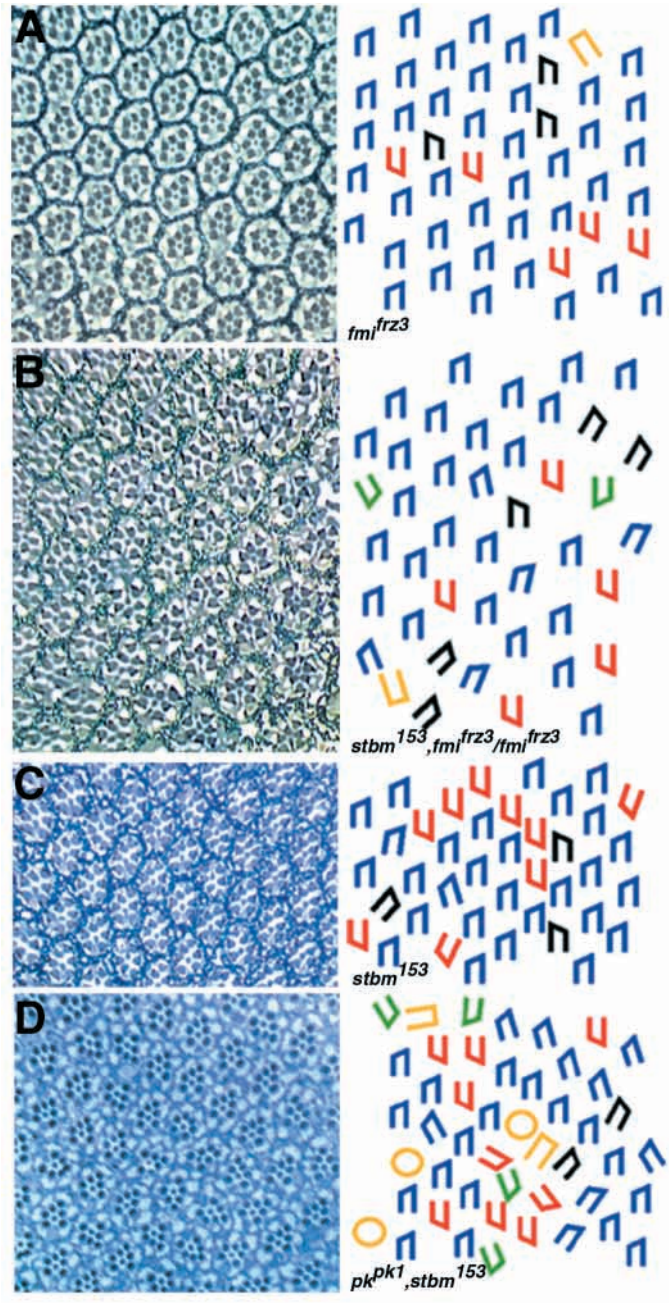

Fig. 2. Genetic enhancement of *fmi* by *stbm* and *stbm* by *pk*. Tangential sections through adult eyes (left) and the corresponding schematics (right). (A) Approximately 12% of ommatidia adopt incorrect polarity in a fmi^{frz3}/fmi^{frz3} hypomorphic mutant. (B) $stbm^{153}$, fmi^{frz3}/fmi^{frz3}. Haploinsufficiency of $stbm^{153}$, a hypomorphic allele of *stbm*, enhances the fmi^{frz3} homozygous phenotype 3 fold. (C) About 40% of ommatidia in a $stbm^{153}/stbm^{153}$ homozygote display defects in polarity (B. K. Grillo-Hill, unpublished). (D) Flies homozygous for both $stbm^{153}$ and pk^{pk1} display an enhanced number of symmetrical defects (yellow) relative to $stbm^{153}$ homozygotes. All sections shown are from the dorsal hemisphere, therefore all trapezoids should be blue. (See Table 2 for quantitative data.) Anterior to the right.

fmi eyes, however this is an artifact of the *EGUF* system (Rawls et al., 2002).]

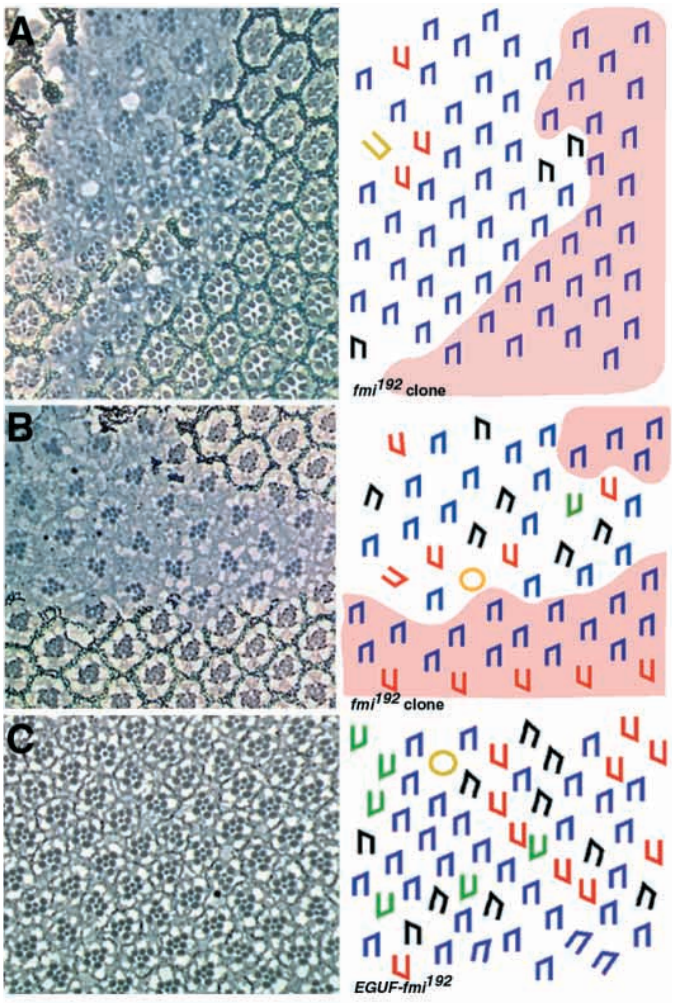

Fig. 3. *fmi* null eyes exhibit a classical ommatidial polarity phenotype. Sections of adult eyes (left) and the corresponding schematics (right). (A,B) fmi^{192} mutant clones have a tissue polarity phenotype. Areas shaded in red represent wild-type tissue; white areas represent mutant clones and include both mutant and mosaic ommatidia. fmi^{192} clones close to the equator (B) have a stronger polarity phenotype. (C) *EGUF-*fmi^{192} eyes, which are completely mutant for *fmi*, also display a typical polarity phenotype. (See Table 3 for quantitative data.) Anterior to the right.

fmi acts autonomously within ommatidia to establish polarity

Gene products that act at a distance generally exert their influence in a non-autonomous fashion, while gene products that exert their effects intracellularly act autonomously. *fmi* has been shown to act autonomously in the wing (Chae et al., 1999). Since tissue-specific differences have been observed in the autonomy of some gene products (for example, *fz)*, we analyzed the polarity of ommatidia in and near *fmi* mutant clones to confirm that *fmi* also acts autonomously in the eye. This analysis demonstrated that the presence or absence of *fmi* does not affect neighboring ommatidia, suggesting that *fmi* acts autonomously within ommatidia. In other words, genetically mutant and mosaic ommatidia have no effect on wild-type ommatidia outside the clone, nor does wild-type tissue rescue ommatidia that are mutant or mosaic for *fmi* (Fig. 3A,B).

Table 4. *fmi* null mutants display a classical tissue polarity phenotype in the eye

Polarity defect	hs-*fmi*^{192} clones	*EGUF-fmi*^{192}
AP	103 (13.0%)	214 (13.3%)
DV	130 (16.4%)	183 (11.4%)
AP+DV	24 (3.0%)	82 (5.1%)
R3/R3	25 (3.2%)	60 (3.7%)
R4/R4	2 (0.3%)	33 (2.0%)
Fail to rotate	6 (0.8%)	40 (2.5%)
Total errors	290 (36.6%)	612 (38.0%)
n	792	1612

Similar findings reported by Das et al. support the autonomous requirement for Fmi in developing ommatidia (Das et al., 2002).

To determine if *fmi* acts in one specific photoreceptor to establish the orientation of an ommatidium, we carried out an analysis of mosaic ommatidia, ommatidia that contain a mixture of wild-type and mutant photoreceptors. We scored these ommatidia to determine the requirement for Fmi in each photoreceptor to direct polarity and found that Fmi is not required in any specific photoreceptor(s) for normal rotation; rather, if at least one photoreceptor expresses *fmi*, the ommatidium can, but not necessarily will, rotate correctly (data not shown). As with *stbm*, proper rotation is only guaranteed when all photoreceptors within an ommatidium are wild type for *fmi*. Das et al. (Das et al., 2002) propose that Fmi function in R3 and R4 is necessary and sufficient for polarity. While this may be true, we cannot rule out the possibility that Fmi may also play a role in the remaining six photoreceptors since we have seen a small fraction of mosaic ommatidia in which both R3 and R4 are wild type for *fmi*, yet these ommatidia still rotate incorrectly (data not shown).

To determine if Fmi is required in any specific photoreceptor for cell fate specification, we examined developmental pairs of photoreceptors (R1/R6, R2/R5 and R3/R4) that were mosaic within the pair. If Fmi is required to specify the R3 photoreceptor, for example, then there would be a trend such that in the majority of mosaic R3/R4 pairs, the photoreceptor that expresses *fmi* would become the R3. We do not see any such trends for any of the pairs, consistent with the findings of Das et al. (Das et al., 2002), suggesting that Fmi is not required for binary photoreceptor fate decisions in developing ommatidia.

Stbm localization is dynamic

Stbm is expressed in a dynamic pattern in the third larval instar. Anterior to, in, and immediately posterior to the morphogenetic furrow, Stbm is uniformly expressed on the apical membranes of all cells (Fig. 4A-C). [In the discussion that follows, row numbers are as defined by Wolff and Ready (Wolff and Ready, 1993); each row is equivalent to 1.5-2 hours of development.] Four to five rows posterior to the furrow, at about the time ommatidial rotation first becomes apparent, Stbm begins to undergo an intriguing change in its pattern of localization. First, it becomes prominent at the membranes of photoreceptors R3 and R4, except where they contact R2 and R5, respectively, while simultaneously dropping to undetectable levels in photoreceptors R8, R2 and R5 [this stage is also described by Strutt et al., using Stbm-YFP (Strutt et al., 2002)]. Second, no protein is detectable at the interfaces between photoreceptors R3/R2 or R5/R4. A restricted region of Stbm staining is evident at the posterior tip of R8 where it contacts R1, R7 and R6, and likely reflects the presence of Stbm in R1, R7 and R6, but not in R8

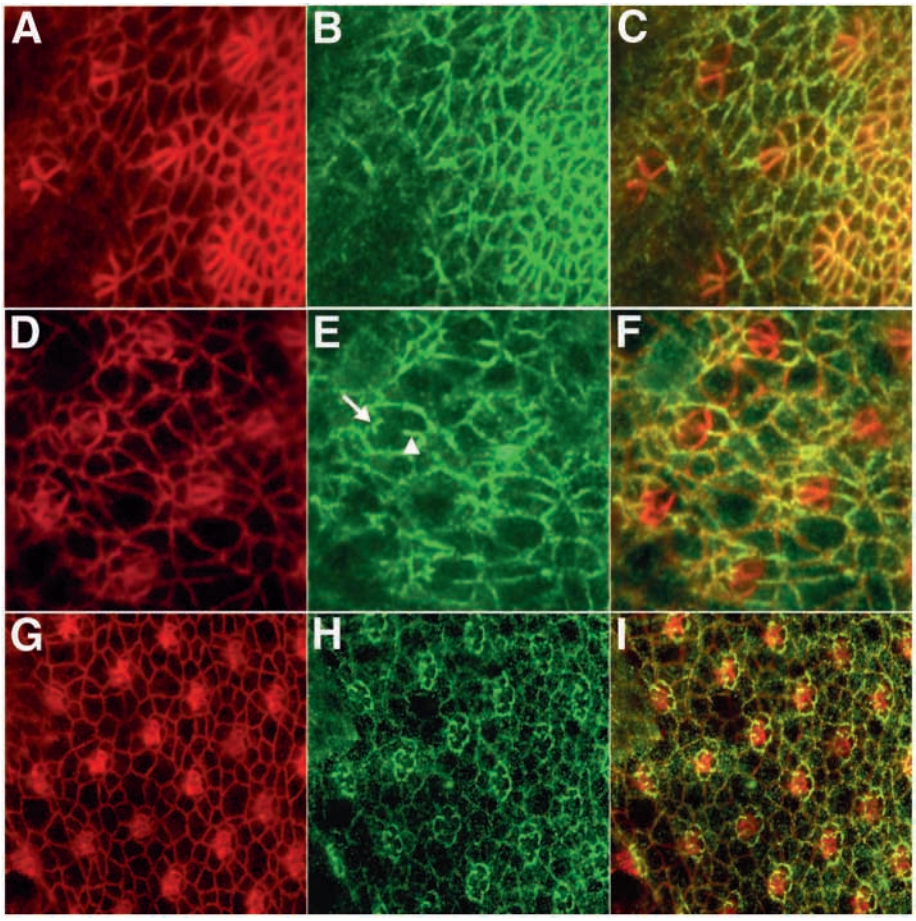

Fig. 4. Stbm localization is dynamic in developing ommatidia. In all panels, anti-Arm, which outlines cells, is shown in red and anti-Stbm is shown in green. (A-C) Stbm is uniformly localized to the apical membranes of cells within, and one to two rows posterior to, the morphogenetic furrow. (D-F) By row 6, Stbm is localized strongly to the anterior membranes of R3 and R4, to the boundary between them (arrowhead), and to the tip of R8 where it contacts R1, R7 and R6 (arrow). Also by this point, Stbm has disappeared from the cell membranes of R8, R2 and R5. (G-I) Posterior region of developing eye imaginal disc showing Stbm localization in the cone cells. See text for details. Anterior to the right.

(Fig. 4D-F). While the level of resolution of these images does not reveal if Stbm is present in only R3 or R4, or in both cells, studies of Stbm-YFP mosaic clones have demonstrated that Stbm is present only in R4 at the R3/R4 boundary (Strutt et al., 2002).

Given that photoreceptors R3 and R4 seem to act as the predominant compass in determining ommatidial polarity in the eye, it is intriguing that Stbm remains abundant at the interface between these two cells. It is equally interesting that Stbm is removed from photoreceptors R8, R2 and R5. At this point it is not known if removal of Stbm from these photoreceptors is essential to achieve normal ommatidial polarity.

Later in development, Stbm is localized in the cone cells. Initially, it is most prominent at the points of contact between the cone cells. It continues to be expressed at high levels in the cone cells once they meet centrally (Fig. 4G-I). The functional relevance of Stbm at these sites is not obvious since cone cell assembly is virtually normal in *stbm* mutant eyes (a small percentage of ommatidia have only three cone cells, but this phenotype may be a secondary effect of improper recruitment by the underlying photoreceptors). No anti-Stbm staining is evident in eye discs that are null for *stbm* (*stbm*^{6cn}) (data not shown).

Fmi and Stbm colocalize early, but not late, in ommatidial development

Fmi co-localizes with Stbm anterior to, within and for several rows posterior to the furrow (Fig. 5A, parts a,b; 5B, parts a,b). [The pattern of Fmi localization was also recently reported by others (Yang et al., 2002; Das et al., 2002; Strutt et al., 2002); here, we extend these observations by providing a developmental time-course for the dynamic distribution of Fmi.] The co-localization persists until approximately seven rows posterior to the furrow, at which point the patterns diverge in two intriguing ways. First, approximately 7-8 rows behind the furrow, Fmi becomes diminished in photoreceptor R3 and simultaneously becomes enhanced in photoreceptor R4 (Fig. 5Ac,Bc). As an intermediate step in this change in protein distribution, Fmi becomes weaker in the polar region of R3, resulting in a transient asymmetry in which Fmi is more prominent in the equatorial region of R3. It is not clear why Fmi undergoes a shift from expression in both R3 and R4 to expression in R4 alone. Perhaps there are Fmi-dependent qualities to being an R4 that cannot be detected in a standard mosaic analysis, such as the placement or morphology of the cell's rhabdomere.

The second way in which Fmi localization differs from that of Stbm is that two to four rows after Fmi becomes conspicuous in R4, Fmi protein becomes internalized into large, punctate structures, whereas Stbm does not (Fig. 5Ad,Bd). These vesicular structures are found in the photoreceptor cell bodies, slightly above the level of the R3 and R4 nuclei. Based on size (approximately 700-800 nm), they resemble multivesicular bodies (MVBs). The majority of these vesicles accumulate centrally within the ommatidium at the junction where photoreceptors R8, R2, R5, R3 and R4 meet, although a small number are evident at the anterior end of the ommatidium in R3 and/or R4. The internalization of Fmi is not essential for rotation, since this event takes place once rotation is well underway.

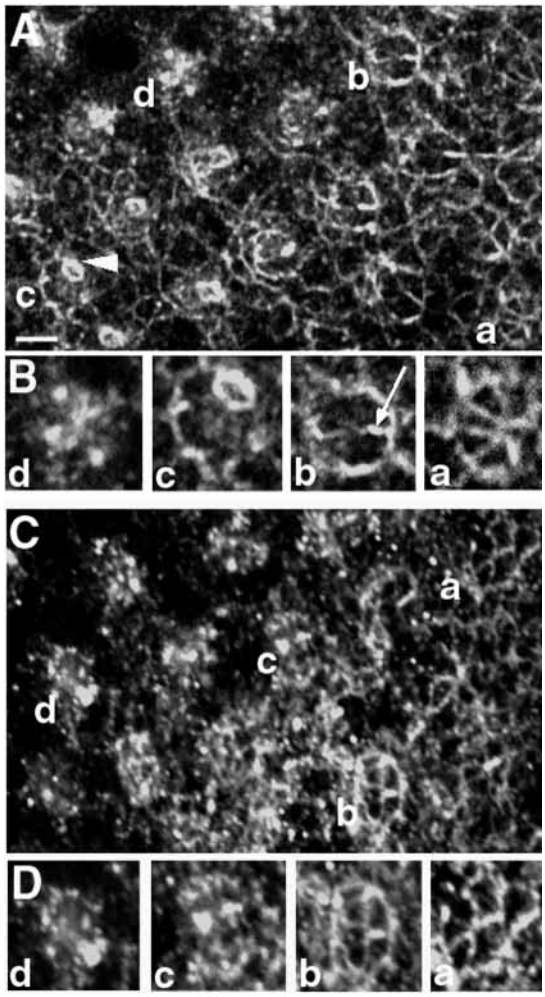

Fig. 5. Fmi localization is dynamic throughout development and is dependent upon *fz*. (A**)** Wild-type third instar eye disc immunostained with anti-Fmi (white arrowhead indicates an R4 cell with a high level of Fmi). (B) High-magnification images of areas a-d in A. (a) Fmi is localized to all membranes of nascent photoreceptors in developing ommatidial clusters. (b) By row 6, Fmi is prominent at the membranes of R3 and R4 (white arrow indicates contact between R3 and R4) and at the point of contact between R1/R7/R6 and R8. (c) By row 8, Fmi is enhanced in R4 and by row 10 appears in punctate structures (d). (C) Fmi localization is disrupted in eye discs homozygous for fz^{KD4A} (a null allele). (D) High-magnification images of areas a-d in C. (a) Fmi localization is unaffected ahead of the furrow (not shown) and in early ommatidial precursors. (b) Localization of Fmi is not affected at this stage. (c) Preferential accumulation of Fmi to R4 is abolished in the fz^{KD4A} background. (d) Vesicle morphology is disrupted, primarily in the number, size and position of Fmi-containing vesicles. Scale bar: ≈ 5 μm. Anterior to the right.

Fmi is processed through the endocytic pathway

The predominance of Fmi-containing vesicles at the junction of photoreceptors R8, R2, R5, R3 and R4 suggested that this internalization may be the means by which Fmi is removed from these cells, or at least from a subset of these cells. In an effort to identify the process underlying this internalization, we tested the efficiency of this process in two mutants that interfere with the endocytic pathway: *shibire* (*shi*) and *hook*

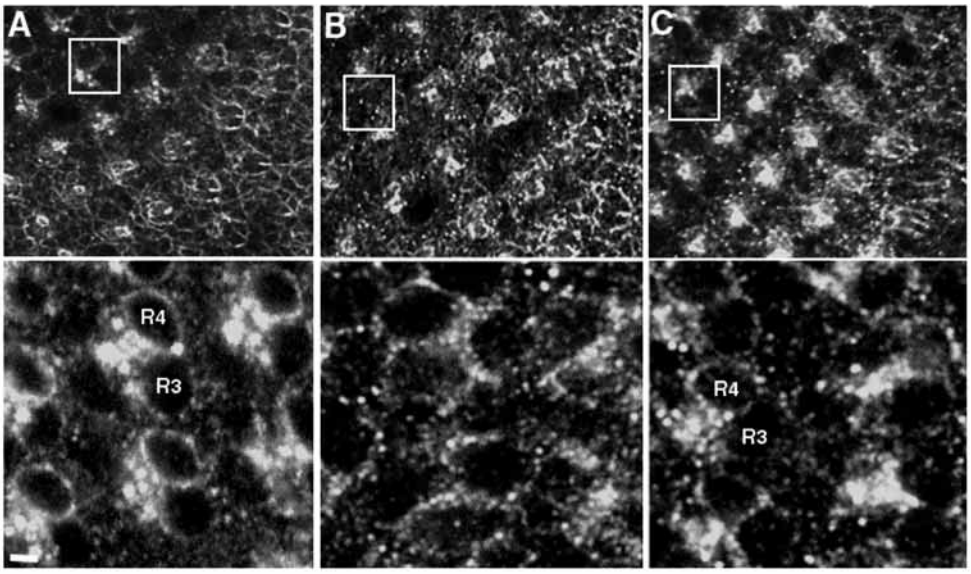

Fig. 6. Fmi is endocytosed. Bottom panels show high magnification images of ommatidia that correspond to the stages represented by the ommatidia in the boxes in top panels. (A) In wild type, Fmi localizes to large vesicles between the nuclei of R3 and R4. (B) In a shi^{2ts} mutant heat-treated for 2 hours, the large vesicles seen in wild type have been replaced by small puncta decorating membranes. (C) In a hk^{11} mutant, the large MVB-like vesicles are also replaced with smaller puncta, although they are larger than those seen in *shi* mutants. Scale bar: ≈ 1 μm. Anterior to the right.

(*hk*). We found that the vesicularization of Fmi is altered in these mutants, indicating that Fmi is internalized via endocytosis.

shi, which encodes the *Drosophila* dynamin, is required early in the endocytic pathway for the budding of clathrin-coated pits from the membrane upstream of the fusion of these structures with endosomes (Chen et al., 1992) (reviewed by Narayanan and Ramaswami, 2001). Temperature-sensitive shi^{2ts} larvae were heat shocked for 1 hour at the restrictive temperature, sacrificed immediately and immunostained with an antibody against Fmi. In shi^{2ts} larvae, the MVB-like, Fmi-containing vesicles normally found in wild type (Fig. 6A) are abolished; Fmi is instead found in small puncta on cell membranes (Fig. 6B). The large Fmi-containing vesicles reappear in larvae allowed to recover for 1-6 hours at room temperature (data not shown).

hk, which encodes a novel component of the endocytic pathway, acts downstream of *shi* in this pathway and is required for the formation and/or maintenance of MVBs (Kramer and Phistry, 1996; Kramer and Phistry, 1999). In hk^{11} mutants, the large, MVB-like vesicles are absent; instead, Fmi is localized to smaller cellular puncta at the junction where the large vesicles normally localize (R8/R2/R5/R3/R4) (Fig. 6C). The failure of Fmi to accumulate in vesicles in *shi* and *hk* mutants suggests that the Fmi-containing vesicles in wild-type eyes result from the endocytosis of Fmi. While the internalization of Fmi into vesicles is dependent on endocytosis, earlier changes in distribution of the protein (for example, its removal from R8, R2, R5 and subsequent accumulation in R4) are not.

The functional significance of Fmi endocytosis in the eye is not known. Clearly, this internalization is taking place too late to initiate or mediate rotation. Perhaps it is necessary for rotation to stop. It could also be important for other aspects of development given that the endocytosis of membrane-associated receptors is required for signaling in key developmental pathways [for example, Notch, Dpp, and Wg (Parks et al., 2000) (reviewed by Narayanan and Ramaswami, 2001)].

The asymmetric localization of Fmi requires Fz and Notch activity

The regulation of Fmi localization in the larval eye disc shows a dependency on *fz* (Fig. 5C,D) (Strutt et al., 2002; Das et al., 2002) and *Notch* (*N*) (data not shown) (Das et al., 2002), genes implicated in R3 and R4 cell fate determination, respectively. The dependency of Fmi localization on *fz* has also been described for Fmi localization in the wing (Usui et al., 1999; Chae et al., 1999).

The early pattern of Fmi localization is unaffected in the absence of Fz – it is still localized to all cell membranes anterior to the furrow (data not shown) and in nascent photoreceptor clusters (Fig. 5Ca,Da). Furthermore, slightly later in development, Fmi is still abundant in photoreceptors R3 and R4. However, whereas Fmi would ordinarily be removed from photoreceptors R8, R2 and R5 at this stage in wild type, it is only partially removed from these cells in the fz^{KD4A} mutant (Fig. 5Cb,Db). The most notable change in Fmi localization is that it no longer accumulates asymmetrically in R4 (Fig. 5Cc,Dc). The size, number and location of Fmi-containing vesicles are also disrupted in fz^{KD4A} larvae: there are more vesicles, they are smaller and they accumulate approximately four rows earlier in development (Fig. 5Cd,Dd). We observe similar defects in Fmi localization in N^{ts1}larvae heat-shocked for 6 hours (data not shown). Additionally, Das et al. (Das et al., 2002) show that Fmi localization is also perturbed when N-mediated signaling is knocked down via overexpression of the *sev-Su(H)-EnR* transgene. While these data do suggest a role for N in the asymmetric localization of Fmi, one cannot yet be assigned, given the abundance of roles for N throughout development.

The observations that *fmi* and *stbm* have similar phenotypes, that they interact genetically and that their products co-localize, suggested that they may act in the same pathway to specify tissue polarity. To explore the possibility that Stbm and Fmi define a complex, we investigated both the localization of Fmi in a null *stbm* background and the localization of Stbm in *EGUF-fmi* eyes. In neither case was the localization affected

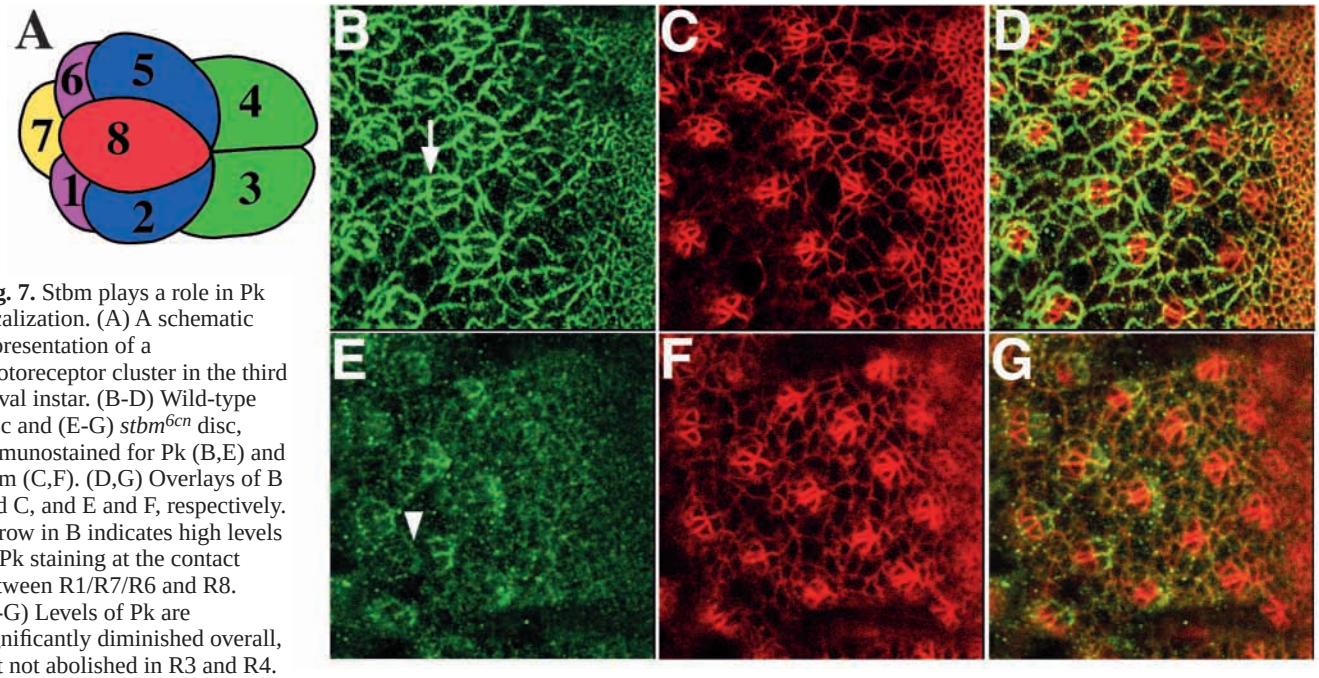

Fig. 7. Stbm plays a role in Pk localization. (A) A schematic representation of a photoreceptor cluster in the third larval instar. (B-D) Wild-type disc and (E-G) *stbm*^{6cn} disc, immunostained for Pk (B,E) and Arm (C,F). (D,G) Overlays of B and C, and E and F, respectively. Arrow in B indicates high levels of Pk staining at the contact between R1/R7/R6 and R8. (E-G) Levels of Pk are significantly diminished overall, but not abolished in R3 and R4. Pk staining at the contact between R1/R7/R6 and R8 is not detectable (arrowhead in E). In all panels, anti-Pk is shown in green and anti-Arm is shown in red. Anterior to the right.

(data not shown), demonstrating that Stbm is not required for Fmi localization, nor is Fmi required for Stbm localization. Furthermore, we have been unable to demonstrate a physical interaction between Fmi and Stbm using co-immunoprecipitation assays (data not shown).

pk and *stbm* interact

In the deficiency screen described earlier, a second tissue polarity gene, *pk*, was identified as a dominant genetic modifier of *stbm*. The original deficiency, Roote 276, which uncovers 42E4-43E7, enhances the *sev-stbm* phenotype from one in which 10% of ommatidia have defects in polarity to one in which 27% have defects (Table 1). The best candidate interactor was *pk*, a tissue polarity gene that maps to 42F2-43A1. We demonstrated that *pk* was the gene responsible for the dominant enhancement of the *sev-stbm* phenotype: haploinsufficiency of *pk*^{pk1}, a *pk* allele with no eye phenotype, enhances the *sev-stbm* phenotype to the same degree as the original deficiency (Fig. 1F; Table 2). We confirmed this genetic interaction in a loss-of-function *stbm* background: the percentage of symmetrical defects in *stbm*^{153}, *pk*^{pk1} double homozygotes is significantly enhanced relative to *stbm*^{153} homozygous flies (Fig. 2C,D; Table 3).

The genetic interaction between *stbm* and *pk* may have its basis in a physical interaction that enhances or stabilizes these proteins at the R3/R4 boundary. To explore this possibility, we examined Stbm localization in a *pk* mutant background, and Pk localization in a *stbm* mutant background. Stbm localization does not appear to be affected in a *pk*^{eq} background (a genetic null that fails to complement *pk*$^{pk\text{-}sple}$ alleles, data not shown). However, Pk localization is disrupted in a *stbm*^{6cn} null background. We have characterized the distribution of Pk in wild-type eye imaginal discs (Fig. 7B-D) and find that it is indistinguishable from that of Stbm (Fig. 4). Pk is significantly reduced overall in the *stbm*^{6cn} background. While some protein does accumulate at the boundary between R3 and R4, Pk is not detectable at the R8/R1/R7/R6 boundary (Fig. 7E-G). Physical interactions have not been demonstrated between either of these proteins, nor have genetic interactions between *fmi* and *pk* been shown. These data are consistent with the possibility that Stbm, Fmi and Pk may all function together in a complex.

DISCUSSION

The proteins encoded by the tissue polarity genes, *fz*, *pk*, *dsh*, *dgo*, *stbm* and *fmi* are thought to make up a dynamically regulated membrane-associated complex. The asymmetric localization of this complex is thought to be required for the regulation of Fz and N activity, which ultimately results in the appropriate specification of photoreceptors R3 and R4 (Strutt et al., 2002; Das et al., 2002). This pathway also regulates the polarization of wing hairs, although there appear to be tissue-specific differences (Tree et al., 2002).

In an attempt to define more precisely the role of Stbm in the tissue polarity pathway, we have identified genetic interactions between *stbm* and two other tissue polarity genes, *fmi* and *pk*. Characterization of the *fmi-stbm* interaction revealed a requirement for Fmi in ommatidial polarity and a dynamic pattern of Fmi localization that depends on Fz and N. We have also raised an antibody against Stbm, characterized its subcellular localization, and shown that the localization of Fmi and Stbm differs in two ways: first, Fmi is enriched in R4, whereas Stbm is not, and second, Fmi, but not Stbm, is endocytosed. Characterization of the *pk-stbm* interaction showed that *pk* enhances the *stbm* phenotype and that Pk localization requires Stbm.

Pk localization requires *stbm* function

Three alternatively spliced transcripts are encoded by the *pk* locus: pk^{pk}, pk^{M} and $pk^{pk\text{-}sple}$. Although these three isoforms differ in the 5′ region, they all contain the single PET and three LIM domains characteristic of the Pk protein (Gubb et al., 1999). PET and LIM domains are thought to mediate protein-protein interactions (Dawid et al., 1998). Isoform-specific mutations in the 5′ region of the transcript result in the pk^{pk} phenotype, affecting only the wing and notum, whereas mutations in the LIM- or PET-encoding domains result in $pk^{pk\text{-}sple}$ alleles, null alleles that affect the eye, legs and abdomen in addition to the wing and notum (Gubb et al., 1999).

Our observation that Pk distribution is altered in a null *stbm* background suggests that its localization is, at least in part, dependent on Stbm. The possibility that Pk localization is mediated directly by Stbm has not yet been explored, but the PET and LIM domains are candidates for domain-specific interactions with Stbm. Disruption of these domains would result in genetic null alleles, consistent with the $pk^{pk\text{-}sple}$ phenotype described above.

Although ommatidial polarity is not affected in individuals carrying the pk^{pk1}allele, this allele enhances the *stbm* eye phentoype. Functional redundancy could account for the ability of *pk* to enhance the *stbm* phenotype such that there is no phenotype when *pk* is knocked out but a reduction in *pk* gene dose can be detected by Stbm. Furthermore, Gubb et al. (Gubb et al., 1999) have indicated that the balance of Pk isoforms contributes to the establishment of tissue polarity. Perhaps this balance is also required for Stbm function.

Atypical cadherins in tissue polarity

Cadherins, or Ca^{2+}-dependent cell adhesion molecules, have traditionally been recognized for their role in adhesion and the resulting tumorous phenotype. Fmi, Fat (Ft) and Dachsous (Ds), members of a class of cadherins that contain a large number of extracellular cadherin domains (atypical cadherins), have recently been shown to contribute to the polarization of ommatidia (Fig. 3) (Das et al., 2002; Strutt et al., 2002; Rawls et al., 2002; Yang et al., 2002). While the ability of cells to adhere to one another is clearly essential for the establishment of polarity within epithelia, recent work suggests the role of cadherins extends beyond adhesion.

Several lines of evidence suggest atypical cadherins may be involved in signaling. For example, Ft is required in the haltere to inhibit DV signaling and *ft* mutants display haltere to wing transformations (Shashidhara et al., 1999). In the fly eye, Ft and Ds have been proposed to be required for the transduction of a dorsal-ventral positional signal via cell-cell relay (Rawls et al., 2002). In addition, Yang et al. (Yang et al., 2002) have shown that gradients of Ds and Four-jointed (Fj) activity may regulate Ft to establish this dorsal-ventral cue. It has been suggested that the combined activities of Ds, Fj and Ft, which appear to be functionally conserved in the wing, leg and abdomen (Ziedler et al., 2000), constitute the ‘elusive’ factor ‘X’ in the morphogen model for tissue polarity (Casal et al., 2002).

The data described here are consistent with the notion that Fmi also plays a role in the intracellular signaling required for the establishment of tissue polarity. Given that Fmi is capable of mediating homophilic association between S2 cells (Usui et al., 1999), its role in signal transduction may be indirect and a consequence of a primary role in cell adhesion. However, *fmi* clones in the eye do not give rise to tumors, nor is the tissue grossly disrupted as has been noted in clones of genes that maintain the integrity of tissue [for example, epithelial phenotypes described for *shg* mutant embryos (Tepass et al., 1996; Uemura et al., 1996)]. Therefore, it is possible that the primary role of *fmi* is not to maintain the integrity of tissue via cell adhesion, but rather to maintain sufficient contact between cells to mediate signaling, or even to signal directly.

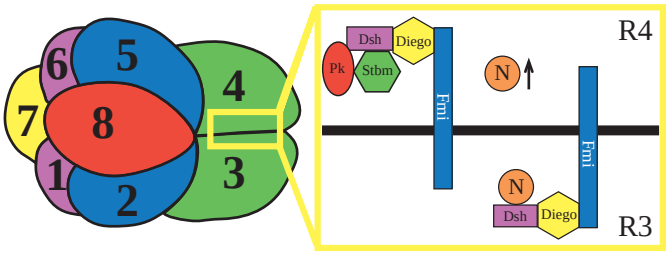

Fig. 8. A model for the asymmetric regulation of N by the tissue polarity proteins. At the junction of photoreceptors R3/R4, Fmi is anchored in both R3 and R4 via homophilic association. In the developing photoreceptor R3, Fmi, Diego, and Dsh form a complex in which N is bound to Dsh. However, in the developing R4, Fmi, Diego, and Dsh form a complex in which Pk and Stbm are bound to Dsh, thereby preventing N from binding to Dsh. Consequently, in R4, N is released from this membrane-bound complex and can signal at high levels.

Model for the regulation of N activity by Stbm, Fmi and Pk

Ommatidial polarization is thought to rely heavily upon the proper specification of two photoreceptors: R3 and R4. Although these two photoreceptors are recruited into the growing ommatidium as a pair and they morphologically resemble one another in early stages of development, they have long been known to be distinct from one another based on their adoption of distinct sets of contacts early in development (Tomlinson, 1985). Recent work on a number of tissue polarity genes provides genetic and molecular evidence that the complexes of tissue polarity proteins are not identical in photoreceptors R3 and R4. The asymmetric regulation of N by these complexes may ultimately lead to low levels of N activity in R3 and high levels in R4, the combination of which is thought to be essential for the specification of the R3 and R4 cell fates.

Fmi has been shown to interact homophilically, and while current data do not establish that Fmi is present in both R3 and R4 at the junction between R3 and R4, in the model that follows, we assume homophilic interactions between the extracellular cadherin domains of Fmi help to anchor Fmi in R3 and R4 on both sides of the R3/R4 interface (Fig. 8). Furthermore, we suggest the intracellular tail of Fmi is involved in signaling, and that it signals through a complex that is made up of at least three proteins: Fmi, Diego (Diego localization depends on Fmi) and Dsh (Dsh co-localizes with Fmi) (Das et al., 2002). Dsh has also been shown to interact physically with two proteins required for R4 specification, N and Stbm (Axelrod et al., 1996; Strutt et al., 2002; Park and

Moon, 2001) and with Pk (Tree et al., 2002). Finally, our *stbm-pk* genetic and protein localization data suggest Pk and Stbm could physically interact within a complex.

As mentioned above, in order to differentially affect signal transduction through the N pathway, the assembly and/or activity of proteins that set up polarity must be different in R3 and R4. The model presented below requires that Stbm and Pk be restricted to the R4 cell to properly modulate N signaling. [Strutt et al. (Strutt et al., 2002) have shown that Stbm is restricted to R4 at the R3/R4 boundary; the subcellular location of Pk in the eye has not yet been determined.]

We propose that the direct interaction between N and Dsh blocks N signaling, and that the different subset of proteins bound to Dsh is the basis of the asymmetry of the complex. In the future photoreceptor R3, N binds Dsh (which is part of the Fmi/Diego/Dsh scaffold) thereby inhibiting N activity in R3 (Fig. 8). In the future R4 cell, where Stbm and perhaps Pk are localized, Fmi, Diego and Dsh also form a complex. However, in this case, the re-organization of the Fmi/Diego/Dsh complex to include Stbm and Pk bound to Dsh may prevent N from binding to Dsh, leading to high levels of N-mediated signaling in R4 (Fig. 8). Ultimately, these differences in gene activity in the R3 and R4 precursors direct the fate specification of these cells.

We express our gratitude to D. Gubb, T. Uemura, H. Kramer, T. Xu and the Bloomington Stock Center for fly stocks; T. Uemura, D. Tree and J. Axelrod for generously providing antibodies; H. Chang and S. Spencer for critical comments on the manuscript; H. Collis for assistance in preparation of the anti-Stbm antibody, and members of the Wolff lab for discussion. T.W. would like to express her gratitude to G. M. Rubin, in whose lab some of this work was initiated. This work was supported by a Lucille P. Markey Pathway fellowship to A.S.R. and NIH grant R01 EY13136 to T.W.

REFERENCES

Axelrod, J. D., Matsuno, K., Artavanis-Tsakonas, S. and Perrimon, N. (1996). Interaction between Wingless and Notch signaling pathways mediated by Dishevelled. *Science* **271**, 1826-1832.

Casal, J., Struhl, G. and Lawerence, P. A. (2002). Developmental compartments and planar polarity in *Drosophila*. *Curr. Biol.* **12**, 1189-1198.

Chae, J., Kim, M. J., Goo, J. H., Collier, S., Gubb, D., Charlton, J., Adler, P. N. and Park, W. J. (1999). The *Drosophila* tissue polarity gene *starry night* encodes a member of the protocadherin family. *Development* **126**, 5421-5429.

Chen, M. S., Burgess, C. C., Vallee, R. B. and Wadsworth, S. C. (1992). Developmental stage- and tissue-specific expression of *shibire*, a *Drosophila* gene involved in endocytosis. *J. Cell Sci.* **103**, 619-628.

Das, G., Reynolds-Kenneally, J. and Mlodzik, M. (2002). The atypical cadherin flamingo links frizzled and notch signaling in planar polarity establishment in the *Drosophila* eye. *Dev Cell* **2**, 6556-6566.

Dawid, I. B., Breen, J. J. and Toyama, R. (1998). LIM domains: Multiple roles as adapters and functional modifiers in protein interactions. *Trends Genet.* **14**, 156-162.

Feiguin, F., Hannus, M., Mlodzik, M. and Eaton, S. (2001). The ankyrin repeat protein Diego mediates Frizzled-dependent planar polarization. *Dev. Cell* **1**, 93-101.

Gubb, D., Green, C., Huen, D., Coulson, D., Johnson, G., Tree, D., Collier, S. and Roote, J. (1999). The balance between isoforms of the prickle LIM domain protein is critical for planar polarity in *Drosophila* imaginal discs. *Genes Dev* **13**, 2315-2327.

Klingensmith, J., Nusse, R. and Perrimon, N. (1994). The *Drosophila* segment polarity gene *dishevelled* encodes a novel protein required for response to the *wingless* signal. *Genes Dev.* **8**, 118-130.

Kramer, H. and Phistry, M. (1996). Mutations in the *Drosophila hook* gene inhibit endocytosis of the boss transmembrane ligand into multivesicular bodies. *J. Cell Biol.* **133**, 1205-1215.

Kramer, H. and Phistry, M. (1999). Genetic analysis of *hook*, a gene required for endocytic trafficking in *Drosophila*. *Genetics* **151**, 675-684.

Lu, B., Usui, T., Uemura, T., Jan, L. and Jan, Y. N. (1999). Flamingo controls the planar polarity of sensory bristles and asymmetric division of sensory organ precursors in *Drosophila*. *Curr. Biol.* **9**, 1247-1250.

Mlodzik, M. (2000). Spiny legs and prickled bodies: new insights and complexities in planar polarity establishment. *BioEssays* **22**, 311-315.

Narayanan, R. and Ramaswami, M. (2001). Endocytosis in *Drosophila*: progress, possibilities, prognostications. *Exp. Cell Res.* **271**, 28-35.

Park, M. and Moon, R. T. (2002). The planar cell-polarity gene *stbm* regulates cell behaviour and cell fate in vertebrate embryos. *Nat. Cell Biol.* **4**, 20-25.

Parks, A. L., Klueg, K. M., Stout, J. R. and Muskavitch, M. A. (2000). Ligand endocytosis drives receptor dissociation and activation in the Notch pathway. *Development* **127**, 1373-1385.

Rawls, A. S., Guinto, J. B. and Wolff, T. (2002). The cadherins, Fat and Dachsous, regulate dorsal/ventral signaling in the *Drosophila* eye. *Curr. Biol.* **12**, 1021-1026.

Shashidhara, L. S., Agrawal, N., Bajpai, R., Bharathi, V. and Sinha, P. (1999). Negative regulation of dorsoventral signaling by the homeotic gene Ultrabithorax during haltere development in Drosophila. *Dev. Biol.* **212**, 491-502.

Stowers, R. S. and Schwarz, T. L. (1999). A genetic method for generating *Drosophila* eyes composed exclusively of mitotic clones of a single genotype. *Genetics* **152**, 1631-1639.

Strutt, D., Johnson, R., Cooper, K. and Bray, S. (2002). Asymmetric localization of frizzled and the determination of notch-dependent cell fate in the *Drosophila* eye. *Curr. Biol.* **12**, 813-824.

Taylor, J., Abramova, N., Charlton, J. and Adler, P. N. (1998). Van Gogh: a new *Drosophila* tissue polarity gene. *Genetics* **150**, 199-210.

Tepass, U., Gruszynski-DeFeo, E., Haag, T. A., Omatyar, L., Torok, T. and Hartenstein, V. (1996). *shotgun* encodes *Drosophila* E-cadherin and is preferentially required during cell rearrangement in the neurectoderm and other morphogenetically active epithelia. *Genes Dev.* **10**, 672-685.

Tomlinson, A. (1985). The cellular dynamics of pattern formation in the eye of *Drosophila*. *J. Embryol. Exp. Morph.* **89**, 313-331.

Tree, D. R., Shulman, J. M., Rousset, R., Scott, M. P., Gubb, D. and Axelrod, J. D. (2002). Prickle mediates feedback amplification to generate asymmetric planar cell polarity signaling. *Cell* **109**, 371-381.

Uemura, T., Oda, H., Kraut, R., Hayashi, S., Kotaoka, Y. and Takeichi, M. (1996). Zygotic *Drosophila* E-cadherin expression is required for processes of dynamic epithelial cell rearrangement in the Drosophila embryo. *Genes Dev.* **10**, 659-671

Usui, T., Shima, Y., Shimada, Y., Hirano, S., Burgess, R. W., Schwarz, T. L., Takeichi, M. and Uemura, T. (1999). Flamingo, a seven-pass transmembrane cadherin, regulates planar cell polarity under the control of Frizzled. *Cell* **98**, 585-595.

Wolff, T. (2000). Histological Techniques for the *Drosophila* eye. Parts I and II. In *Drosophila Protocols* (ed. M. A. W. Sullivan and R. S. Hawley), pp. 201-244. Cold Spring Harbor, NY: Cold Spring Harbor Laboratory Press.

Wolff, T. and Ready, D. F. (1993). Pattern formation in the *Drosophila* retina. In *The Development of Drosophila melanogaster* (ed. M. Bate and A. Martinez Arias), pp. 1277-1325. Cold Spring Harbor, NY: Cold Spring Laboratory Press.

Wolff, T. and Rubin, G. M. (1998). *strabismus*, a novel gene that regulates tissue polarity and cell fate decisions in *Drosophila*. *Development* **125**, 1149-1159.

Xu, T. and Rubin, G. M. (1993). Analysis of genetic mosaics in developing and adult *Drosophila* tissues. *Development* **117**, 1223-1237.

Yang, C., Axelrod, J. D. and Simon, M. A. (2002). Regulation of Frizzled by Fat-like Cadherins during planar polarity signaling in the *Drosophila* compound eye. *Cell* **108**, 675-688.

Zheng, L., Zhang, J. and Carthew, R. W. (1995). *frizzled* regulates mirror-symmetric pattern formation in the *Drosophila* eye. *Development* **121**, 3045-3055.

Ziedler, M. P., Perrimon, N. and Strutt, D. I. (2000). Multiple roles for *four-jointed* in planar polarity and limb patterning. *Dev. Biol.* **228**, 181-196.